Journal of Environmental Chemical Engineering 9 (2021) 104781

Contents lists available at ScienceDirect

Journal of Environmental Chemical Engineering

journal homepage: www.elsevier.com/locate/jece

New polysulfone microcapsules containing metal oxides and ([BMIM][NTf_2]) ionic liquid for CO_2 capture

Muhammad Nisar [a], Franciele L. Bernard [b], Evandro Duarte [b], V.V. Chaban [c], Sandra Einloft [a,b,*]

[a] Post-Graduation Program in Materials Engineering and Technology, Pontifical Catholic University of Rio Grande do Sul – PUCRS, Brazil
[b] School of Technology, Pontifical Catholic University of Rio Grande do Sul PUCRS, Brazil
[c] P.E.S., Vasilievsky Island, Saint Petersburg, Leningrad Oblast, Russian Federation

ARTICLE INFO

Editor: Zhang Xiwang

Keywords:
Ionic liquid
Polysulfone
Microcapsule
Metal oxide

ABSTRACT

CO_2 emission from flue gas is one of the main sources of global warming. The development of new materials with enhanced CO_2 adsorption is crucial to foster sustainable development. In this work, 1-Butyl-3-methylimidazolium bis(trifluoromethylsulfonyl)imide ([bmim][NTf_2]) ionic liquid (IL) was synthesized and combined to metal oxides (Fe_2O_3, CuO and TiO_2) for further encapsulation in polysulfone (PSF) using emulsification method. Computational study using "ab initio" method was also performed. Scanning electron microscopy evidenced the uniform formation of the IL/metal oxide encapsulated polysulfone microcapsule. Transmission electron microscopy (TEM) and Scanning electron microscopy indicates the formation of microcapsules of around 1.0 μm containing a dense core (IL/metal oxide) when Fe_2O_3 was encapsulated by a polymer shell presenting better CO_2 sorption compared to microcapsule containing CuO and TiO_2. Thermogravimetric analysis (TGA) presents microcapsule thermal behavior indicating microcapsule lower degradation temperature when compared to neat PSF. IL encapsulation capacity was determined using acetone immersion test. Results indicated around 40 % of encapsulation capacity. Differential scanning calorimetry shows the complete disappearance of the IL (at -3.14 □) characteristic peak after the acetone immersion test confirming IL removal by the method. The residue wt.% calculated by TGA in air atmosphere was used to determine the metal oxide amount incorporated in the microcapsules. The CO_2 sorption capacity of microcapsule with Fe_2O_3 shows an enhancement of around 47 % as compared to the neat-PSF. Here we reported the development of an effective solvent-free adsorbent for CO_2 capture fostering industrial application.

1. Introduction

Burning of fossil fuels for energy production is triggering a number of environmental issues such as rising of see level and repeated risky weather events. Fossil fuel incineration for power generation accounts for about 40 % of global CO_2 emission [1]. The main source of energy supply in the near future will remain fossil fuels and the CO_2 emission from fossil fuel-fired power plants will continuing being of primary significance [1]. In the last few decades, several CO_2 separation technologies have been developed and practiced to separate the CO_2 from flue gas streams for further transportation. CO_2 production takes place during the combustion process being essential to take into consideration the used technology for selecting a proper CO_2 removal system. According to the available data of technologies for CO_2 capture existing in the market a total cost of around 70–80 % of the power generation process is attributed to carbon dioxide capture and storage (CCS), which is considered costly [2]. However, extensive R&D efforts are concentrated to develop cost-effectively and lower energy penalty technologies.

Liquid solvents mainly perform CO_2 capture from gas stream. This process is the most mature method for CO_2 separation and solvent regeneration occurring mainly by heating. [3] Chemical absorbent for isolating CO_2 from industries and power plant flue gas is one of the main choice. [4,5] Typical solvents are diethanolamine (DEA), Monoethanolamine (MEA) and potassium carbonate. Amine degradation is one of the most important drawback of this technology causing several problems such as equipment corrosion, solvent loss and most serious producing volatile degradation components. Yet, amine emission has a harmful impact on the human environment and health potentially degrading to nitramines and nitrosamines [6,7]. The use of amine scrubbing technology is in front of challenges. Besides the drawback

* Corresponding author at: Post-Graduation Program in Materials Engineering and Technology, Pontifical Catholic University of Rio Grande do Sul – PUCRS, Brazil.
E-mail address: einloft@pucrs.br (S. Einloft).

https://doi.org/10.1016/j.jece.2020.104781
Received 22 September 2020; Received in revised form 28 October 2020; Accepted 12 November 2020
Available online 30 November 2020

already discussed the energy consumption is also a barrier to overcome. Thermal efficiency of a plant is reduced by 20–30 % following 50–80 % rise in the electricity consumption by the incorporation of amine based plant in a post combustion capture (PPC) facility [8]. As the amine regeneration required a heat of around 50 % of the PCC energy consumption, further research should be carry out in the prior bases for its reduction.

Aiming to overcome the amine drawbacks the use of ammonia, piperazine and ionic liquids as solvents have attracted the consideration of researchers. [6,9–14] Ionic liquids (ILs) unique properties appears as an interesting option for CO_2 capture presenting tunable reaction enthalpy with CO_2 and insignificant volatility [15,16]. The severe mass transfer restriction due to the high viscosity of the ILs is the main challenge for CO_2 capture utilization [17]. The loading of the ILs in porous solid material like carbon, silica, and polymer have been introduced to overcome these tasks [18–20]. Encapsulation of ILs increases CO_2 uptake by increasing sorbent specific surface area in the gas separation step enhancing uptake kinetics in contrast to the neat IL. Parlomer et al. [21] reported the use of phenol-formaldehyde resin for the preparation of carbon capsule shells impregnated with IL solution. Results showed a strong increase in the NH_3 gas uptake compared to the pure IL. Lemus et al. [22] described NH_3 and CO_2 absorption/desorption using the same material. Improvement of CO_2 absorption using hybrid capsule containing a core of IL and shell of alkylated graphene oxide and polyurea was reported by Huang et al. [23]. These works clarify that the ILs encapsulation is favorable for overcoming the existing restrictions for their use in CO_2 separation.

The introduction of metal to facilitate amine-based PCC regeneration was described elsewhere. Stern et al. [24] investigated ethylenediamine (EDA) solution in order to regenerate the amine presenting (Cu) ion by electrolytic cell. However, the method is expensive as the deposition of the cupric ion on the electrode consume large amount of electricity. A recent work showed a decrease of 7.8 % in the regeneration thermal energy of the absorbent by adding a slight quantity of Cu ions into amine solution causing the multi-ion effect increasing the mass and heat transfer of amine solution. [25]

The major drawbacks associated with the use of metals ions is its catalytic amine oxidative degradation resulting in amine solution degradation. Experimental application showed that metals dissolved from the stainless steel pipes and packing (chromium (Cr), manganese (Mn), copper (Cu), iron (Fe), vanadium (V) and nickel (Ni)) catalyzed an oxidative degradative effect on the amine solution during the CO_2 capture. [26,27] However, the use of metal oxides for CO_2 capture has well-established advantages combining with the CO_2 present in the flue gas to form carbonates. Heating regenerates the metal oxide resulting in an almost pure CO_2 stream. Essential parameters for selecting a potential metal oxide include their CO_2 capture capacity, absorption rate, thermal stability, regeneration heat cost, and structural properties. Another good advantage of using metal oxides for CO_2 separation is their low cost and abundance in nature. [28] Cheng et al. [1] reported a decrease of 13−24% (depending on the concentration of the Cu ion) in desorption heat of monoethanolamine resulting from a metal-amine complexation.

In this work we focus in the combination of the use of ionic liquids and different metal oxides (Fe_2O_3, CuO and TiO_2) encapsulated in a polymer matrix for CO_2 capture. The obtained nanocapsules or microcapsule were characterized and the effect of the different metal oxides on CO_2 sorption capacity was evaluated. We also investigated the recyclability behavior of microcapsules containing iron oxide and IL for CO_2 capture.

2. Experimental

2.1. Materials

1-Methylimidazole (≥ 99 %, Sigma-Aldrich), acetonitrile (P.A, Synth), Bis(trifluoromethylsulfonyl)amine lithium salt (99.95 % Sigma-Aldrich), 1-chlorobutane (99 %, Sigma-Aldrich), Polysulfone (average Mw ~35,000 by LS, average Mn ~16,000 by MO, pellets, Sigma-Aldrich), dichloromethane (P.A, Synth), gelatin (Sigma-Aldrich), Metal oxide (J.T.Baker) and Polyvinyl alcohol (PVA, Sigma-Aldrich) were used as received.

2.2. [bmim][NTf_2] synthesis

1-Butyl-3-methylimidazolium bis(trifluoromethylsulfonyl)imide ([bmim][NTf_2]) IL was synthesized in a three-necked flask at 80−90 °C during 24 h using 8.21 g (0.1 mol,) of 1-methylimidazole and 13.9 g (0.15 mol) of 1-chlorobutane in acetonitrile following procedures adapted from literature [29](Fig. 1). The volatile material was removed under vacuum (10^{-3} mbar) at the end of the reaction. [bmim] [Cl] was re-dissolved in acetonitrile and gradually added to solution of toluene forming [bmim] [Cl] in the form of solid crystals. The solid crystals were dried under vacuum. Ultimately, the dissolution of 17.5 g (0.1 mol) of [bmim] [Cl] and 28.7 g (0.1 mol) of Bis(trifluoromethylsulfonyl)amine lithium salt in a three-necked flask in 50 ml of distilled water was carried out. The 24 h reaction at room temperature and constant stirring was concluded. Finally, the removal of water under vacuum (10^{-3} mbar) is operated to afford [bmim][NTf_2] IL.

The IL structure was identified by Fourier-Transform Infrared (FTIR) and Proton Nuclear Magnetic Resonance (^{1}H NMR) spectroscopic techniques. The peaks of ^{1}H NMR spectrum (Figure S1) showed the signals of [bmim][NTf_2] IL. ^{1}H NMR (400 MHz, CDCl3) δ ppm: 0.96 (3H, t, −CH3), 1.35 (2H, m, −CH2−CH3), 1.85 (2H, m, −CH2−CH2−CH2), 3.9 (3H, s, CH3-N), 4.16 (2H, t, -N−CH2−CH2), 6.90 (1H, s, −CH), 7.03 (1H, s, −CH) and 8.7 (1H, s, −CH) [30,31]. [Bmim][NTf_2] FTIR spectrum (Figure S2) revealed characteristic peaks of IL [32,33]. The peaks in the range from 2800 to 3200 cm^{-1} are attributed to the C—H stretching vibrations of butyl chain and the methyl group attached to the imidazolium ring. The band at around 1582 cm^{-1} corresponding to C—N symmetric and assymetric stretching of imidazolium ring and peaks at around 791 cm^{-1} and 738 cm^{-1} are associated to the S—N—S group of NTf_2 anion.

2.3. Capsule preparation

IL encapsulation was performed using experimental procedures adapted from literature [34–36]. [bmim][NTf_2] IL (1.2 g) and polysulfone (1.0 g) were dissolved in 20 ml of dichloromethane, different wt. % metal oxide were also added. Then, the mixture was added to aqueous solution containing 0.8 wt% gelatin and a known amount of PVA (1.4 wt.%). The mixture was emulsified for 300 s by stirring using Ultra-turrax (speed range 23,000 rpm). The capsules were collected and the product was washed several times with distilled water. Dried encapsulated IL containing metal oxide were obtained at constant temperature of 25 °C, and subjected to further characterization.

2.4. Molecular modeling

Geometries of individual molecules, ions, and nanoparticles as well as their complexes with carbon dioxide were optimized by means of the steepest-descent algorithm. The procedure was repeated until the energy difference between two consequent multi-atomic configurations became smaller than the requested difference. The convergence threshold was set to 2.1 kJ mol^{-1}. This is significantly smaller than all interaction (binding) energies herein reported. The wave function approximations were derived using the M11 exchange-correlation density functional. [37] Therefore, the calculations reported are based on the meta-GGA approximation. The valence electrons were treated explicitly, whereas the core electrons were modeled by the so-called core potentials. The Los Alamos double-zeta LANL2DZ basis set [38] was used to represent all electrons. The wave energetic function convergence criterion was set to 10^{-6} Hartree.

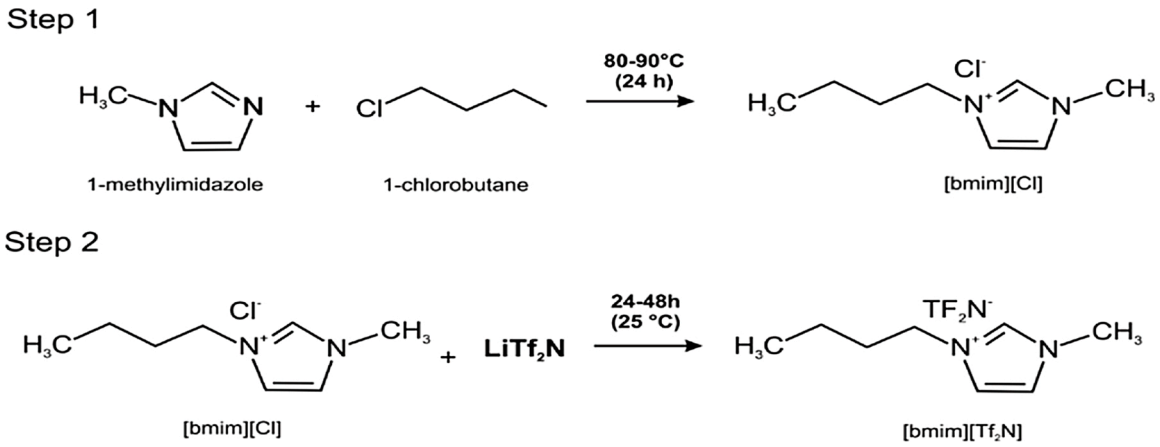

Fig. 1. Synthesis steps of [bmim][NTf_2] IL [29].

For each sorbent component, the interaction energy with CO_2 in the optimized configuration was computed. The basis set superposition energy was excluded from the binding energy using the standard counterpoise methodology. Each reported adsorption energy includes a weak London attraction component thanks to empirical van der Waals correction. [39] The calculations were performed using the GAMESS-2014 code along with in-home procedure [40].

2.5. Characterization of materials

Microcapsule samples structures were identified by Fourier-transform infrared (FTIR). FTIR spectra were recorded on a Perkin-Elmer Spectrum 100 spectrometer in ATR (Attenuated Total Reflection) mode. Samples morphology was determined with a field emission scanning electron microscope (FESEM) using Inspect F50 equipment (FEI Instruments) in secondary electrons mode and transmission electron microscopy (TEM) using a Tecnai G2 T20 FEI operating at 200 kV. Differential Scanning Calorimetry (DSC) thermograms were attained by using differential calorimeter (TA Instruments model Q20). The heating rate of 10 °C min^{-1} from -25 to 200 °C using a nitrogen atmosphere for polymer and encapsulated IL samples. Thermogravimetric analysis (TGA) were performed in a TA model SDT Q600 equipment. The sample was heated up from 20 °C to 800 °C under inert N_2 (20 °C min^{-1}) as well as in the air atmosphere (up to 1000 ℃), the metal amount in the microcapsule was calculated from the TGA residue in air atmosphere, where the residue of the Pure PSF was subtracted from the residue of the microcapsule. IL loading in shell (denoted as IL%) was obtained by acetone extraction method [34,41]. The experiments were carried out in triplicate. Sample was dried for 4 h at 70 °C, weighed (W_1), fully grounded in a mortar and immersed in solvent (acetone) for 48 h. Acetone was able to dissolve completely only IL. Then, the polymer (PSF) was filtrated, dried (4 h at 70 °C) and weighed (W_2). IL loading in shell (IL%) was calculated using Eq. (1).

$$IL\ \% = \frac{w_1 - w_2}{w_1}\ x\ 100 \tag{1}$$

The pressure-decay technique determined CO_2 sorption capacity. The dual-chamber gas sorption cell was similar to Koros et al. [42]. Before measurements, 0.7 g–1 g of the sample was weighed and dried for 1 h at 70 °C (343.15 K). CO_2 sorption experiments were carried out at 45 °C (318.15 K) and 4 bar. CO_2 sorption capacity was calculated using Eqs. (2) and (3).

$$n_{CO2} = \frac{p_i V_{gc}}{Z_{(P_i,T_i)} RT_i} - \frac{p_{eq}(V_t - V_p)}{Z_{(p_{eq},T_{eq})} RT_{eq}} \tag{2}$$

$$w_{CO2/g} = \frac{n_{CO2} M}{W_s} \tag{3}$$

Here, $w_{CO2/g}$ is the weight of gas adsorbed by the sample, p_i and T_i give the pressure and the temperature in the gas chamber, respectively; those parameters at equilibrium are represented as p_{eq} and T_{eq}; V_{gc} is the gas chamber's volume, V_p is the volume of the sample, and V_t is the total volume of the sorption cell; the coefficient of compressibility "Z" for CO_2 is obtained via Span-Wagner equations of state [43].

3. Results and discussion

3.1. FTIR analysis of the synthesized microcapsule

Fig. 2 presents typical FTIR spectra of IL/PSF/metal oxide encapsulated samples exemplified by PSF-IL-Fe_2O_3-20 %; PSF-IL-TiO_2-20 % and PSF-IL-CuO-20 % samples. The spectra showed characteristic peaks of PSF [34,36] at ~1582, ~1505 and ~1486 cm^{-1} (aromatic rings stretching), at ~1238 (S═O asymmetric stretching) and ~1145 cm^{-1} (C—O—C). Peaks attributed to [bmim][NTF_2] IL [32,33] can be seen at 3200 – 2800 cm^{-1} (C—H aromatic stretching imidazol ring), ~1582 cm^{-1} of CH_2-N, CH_3-N (symmetric and asymmetric stretching, respectively), ~791 and 738 cm^{-1} (S—N—S group) of NTf_2^- anion confirming IL encapsulation within a polysulfone shell.

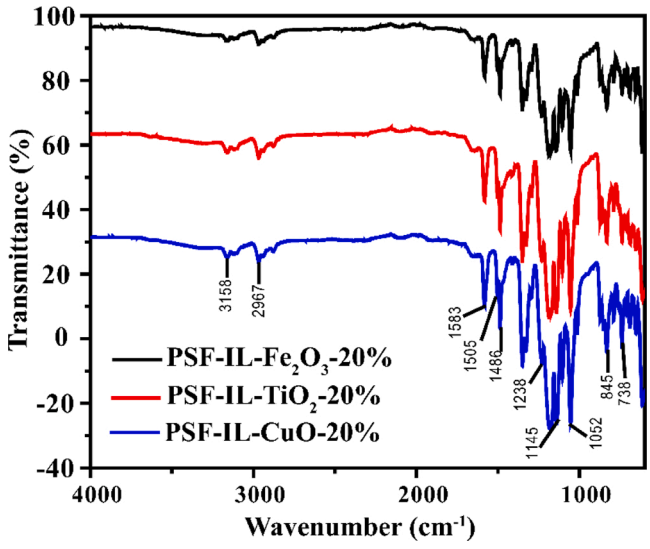

Fig. 2. FTIR spectra of PSF encapsulated [bmim][TF_2N].

3.2. Morphological characterization

Microcapsules structure and formation were depicted by scanning and transmission electron microscopy. Fig. 3 shows the SEM micrographs of synthesized microcapsules with different amount of iron oxide. It can be seen that the obtained microcapsule are uniform and in the range of around 1 μm with the addition of all iron oxide content. However, a more uniform structure was observed in case of 10 wt.% of the iron oxide as seen in Fig. 3 (C) and (D). The micrographs show uniform distribution of the microcapsule with low agglomeration.

Fig. 4 shows SEM images of microcapsules containing CuO and TiO_2. Unlike microcapsules obtained using Fe_2O_3 one can observe agglomerated and high sized microcapsules when using CuO and TiO_2 as metal oxides. It can be inferred that CuO and TiO_2 incorporation do not favor uniform microcapsule formation at the same synthesis condition of Fe_2O_3. Microcapsule size is bigger using 2 wt.% of TiO_2 compared to the sample containing 2 wt.% of CuO (compare Fig. 4 (a) and (d)). Increasing CuO content an opposite behavior was observed obtaining high sized microcapsules compared to TiO_2 (compare Fig. 4 (b), (c) and (e), (f)).

Transmission electron microscopy (TEM) images of the microcapsule containing different amount of iron oxide are presented in Fig. 5. The microcapsule shows a dense centered part attributed to the IL and a thin polymeric partition surrounding the dense part. For a low iron oxide amounts of 2 wt.% (Fig. 5 (A) and (B)) it is difficult to see the presence of the metal oxide in the capsules. For a higher amount of iron oxide (10 wt.% and 15 wt.%), it can be seen the Fe_2O_3 in the images as small agglomerates.

Fig. 6 presents TEM images of microcapsule containing CuO and TiO_2. It can be seen that using 2% of CuO a rather uniform capsule was formed (Fig. 6 (a) and (b)). Whereas, increasing the amount of CuO to 20 % inhomogeneous capsules were obtained (Fig. 6 (c)). Similarly, inhomogeneous and agglomerated microcapsules was formed using TiO_2 as metal oxide (Fig. 6 (d), (e) and (f)). The existence of black irregular spots inside and outside of capsule indicates the presence of the metal oxide.

3.3. Thermal analysis

PSF, pure IL, and microcapsule thermal stability were investigated by TGA under nitrogen atmosphere (see Fig. 7 and Table 1). The maximum degradation temperature of IL and PSF was 480 °C and 545 °C respectively. Residual weight of the pure PSF in the nitrogen atmosphere was 32.4 % at 700 °C. The high residual weight is probably due to the existence of the aromatic moiety in the PSF backbone producing thermally stable carbonaceous constituents during PSF degradation. [36] The initial degradation of the IL started at 447 °C and attained maximum degradation at 480 °C. The microcapsule initial thermal degradation start at lower temperature around 323 °C with a smaller slope when comparing to the pristine IL indicating the IL successful encapsulation by the polymer matrix. Thermal stability of the absorbent is an important factor to be considered when designing a new sorbent. The residual weight of the microcapsules (PSF-IL-Fe_2O_3-2%, PSF-IL-Fe_2O_3-10 %, PSF-IL-Fe_2O_3-15 %, PSF-IL-TiO_2-2%, PSF-IL-TiO_2-15 %, PSF-IL-TiO_2-20 %, PSF-IL-CuO-2%, PSF-IL-CuO-15 %, and PSF-IL-CuO-20 %) were 16 %, 23 %, 24 %, 12 %, 22 %, 15 %, 16 %, 22 % and 26 % respectively, whereas the maximum degradation was observed around 446 °C–464 °C for all microcapsule as seen in Table 1. The lower residual wt.% as compare to pure PSF (32.4 %) indicates the ionic liquid encapsulation inside the PSF core shell. Microcapsule lower degradation temperature when compared to the IL and pure PSF (see Fig. 7) is attributed to the metal ion presence acting as catalyst of polymer degradation starting microcapsule degradation at relatively lower temperature. Similar catalytic activity of metal ions for polymer degradation was described elsewhere [44–46]. After acetone immersion test the TGA thermograms (see Fig. 7 B) shows identical initial degradation as that of the microcapsule but final degradation and residual mass very similar to the pure PSF. Besides, the samples containing 15 % of Fe_2O_3, 20 % of CuO and 20 % of TiO_2 shows superior residual mass compare to the neat PSF due to the presence of higher metal oxide amount. The lower initial degradation of the shell material after the acetone immersion test can be explain by the catalytic effect of the metal oxides as mentioned above. It can be

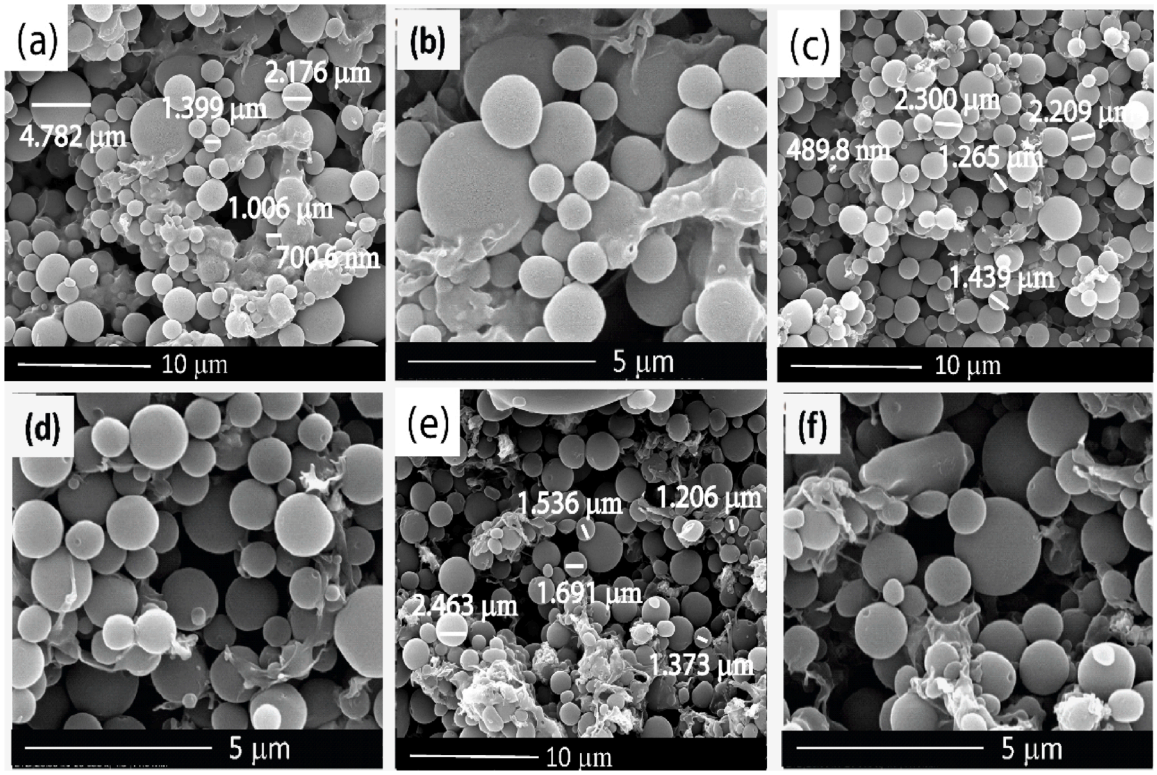

Fig. 3. SEM images of the microcapsule containing different wt.% of Fe_2O_3 (A) and (B) 2.0 wt.% of Fe_2O_3 (C) and (D) 10 wt.% of Fe_2O_3 (E) and (F) 15 wt.% of Fe_2O_3.

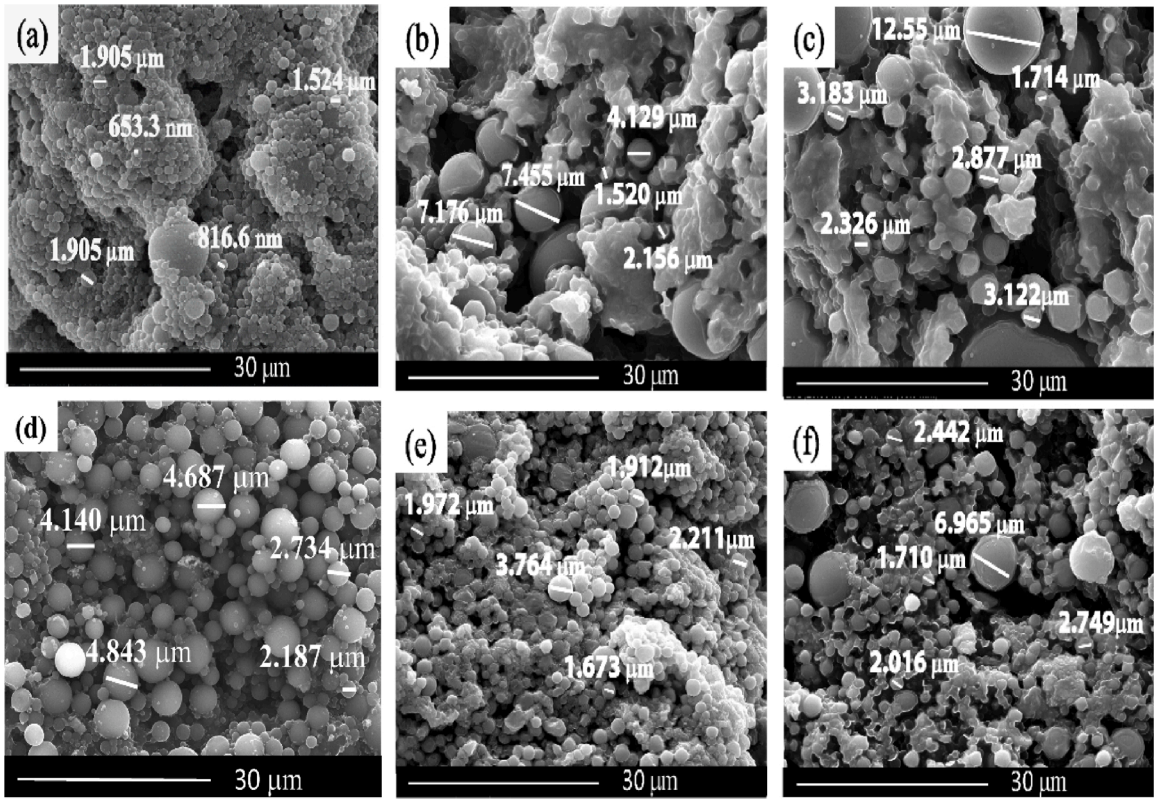

Fig. 4. SEM images of the microcapsule containing CuO-2% (a), CuO-15 % (b), CuO-20 % (c) TiO_2-2% (d), TiO_2-15 % (e) and TiO_2-20 % (f).

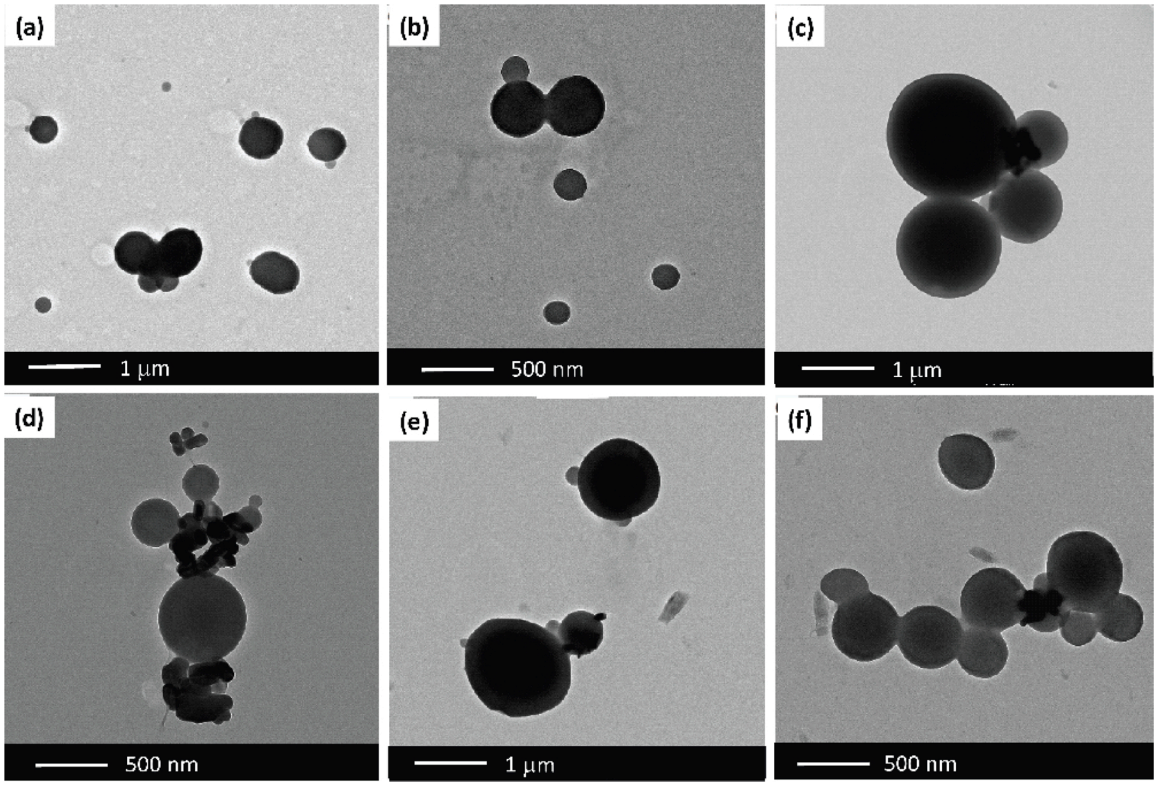

Fig. 5. TEM images of microcapsule containing different amount of Fe_2O_3 (A),(B) 2 wt % of Fe_2O_3 (C), (D) 10 wt % of Fe_2O_3. (E), (F) 15 wt % of Fe_2O_3.

noted from the TGA thermograms that all the microcapsule show a similar trend of thermal degradation starting at around 323 °C and reaching a maximum value of around 464 °C.

Metal oxide wt.% was obtained by TGA at 1000 °C in air atmosphere using neat-PSF and microcapsules samples (see Fig. 8) TGA thermograms. Fig. 8 and Table 1 shows that the TGA residue is not fully in

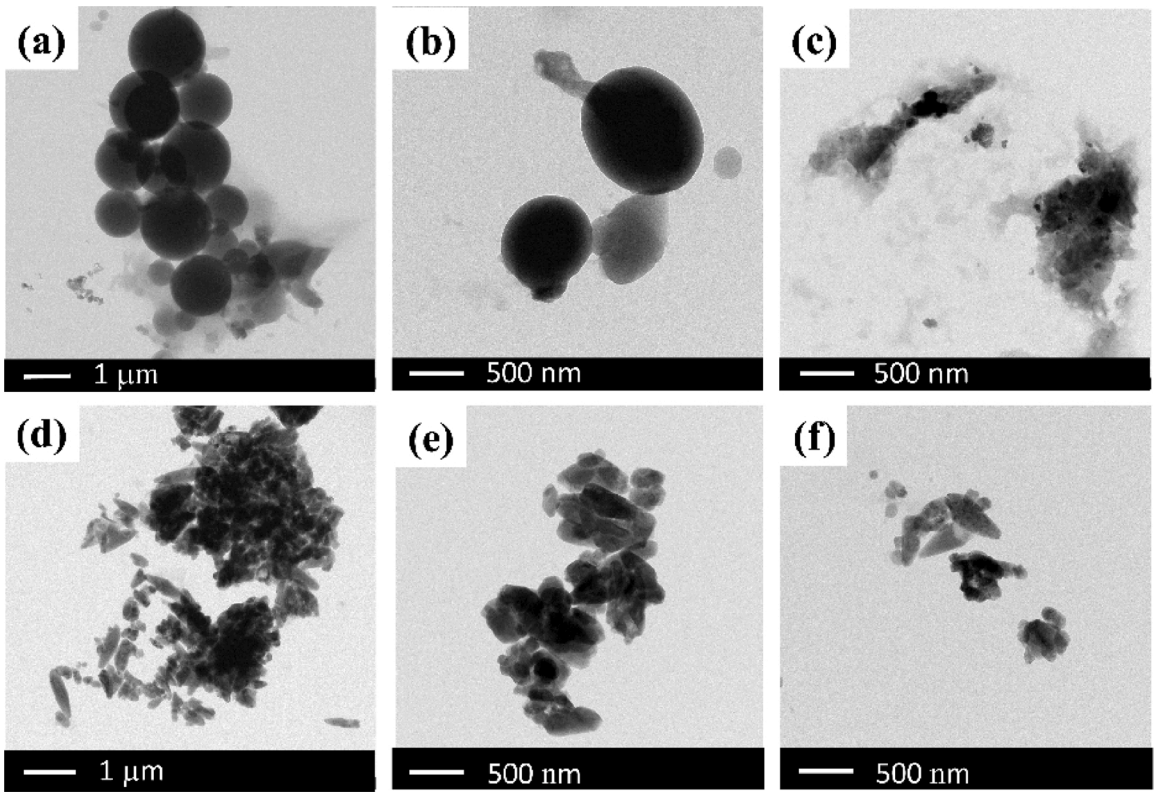

Fig. 6. TEM images of microcapsule containing CuO 2% (a), (b) and 20 % (c), TiO_2 2% (d), (e) and 20 % (f).

agreement with the theoretical amount of the metal oxide incorporated. The amount of the metal oxide was not encapsulated 100 % being the remaining amount of metal oxide removed during microcapsule washing with distilled water after the synthesis.

IL DSC curve presents a melting point at -4.9 °C, and crystallization temperature at -27.2 °C as seen in inset of Fig. 9 (A). All microcapsule showed the melting point at around (-3.4 °C) and crystallization temperature at (-24.7 °C) except the sample with CuO 2% showing a slight different trend of melting (2.4 °C) and crystallization temperature (-18.7 °C) (Fig. 9 A, C and E). Melting and crystallization temperatures values increased compared with non-encapsulated IL probably due to encapsulation of IL in amorphous polymer. This behavior has been reported to encapsulated drugs [47]. A decrease (from 187 °C to 137 °C) in glass transition temperature (T_g) of encapsulated IL was also observed comparing to neat PSF indicating greater microphase separation [48]. Chen et al. [49] reported a similar decrease in T_g of the IL-polymer composite. The introduction of 1-Ethyl-3-Methylimidazolium tetrafluoroborate ([EMIM][BF_4]) and 1-Ethyl-3-Methylimidazolium dicyanamide ([EMIM][DCA]) into cellulose triacetate (CTA) decreased the T_g temperature of the CTA from 198 °C to 11 °C for sample containing 50 wt.% of IL. Their results show a decrease in the CTA crystallinity and increase in the diffusivity and permeability through the membrane [50]. IL into polymeric structure act as a plasticizer to improve chain flexibility, facilitating motion and consequently reducing *Tg* of the polymer [48]. These results evidenced the contribution of all the components in microcapsule formation.

3.4. Quantification of encapsulation (%)

Acetone immersion method adapted from literature [34] was used in order to quantify the encapsulation capacity (IL%). The encapsulation capacity for all microcapsule was around 27%–40 %. Table 2 shows that the higher amount of metal oxide (Fe_2O_3 and TiO_2) results in IL lower encapsulation capacity. Contrary, microcapsule containing CuO shows a reverse effect on the encapsulation capacity. Increasing CuO content from 2% to 20 %, increases IL encapsulation capacity from 32 % to 36 % respectively, as clear from Table 2. A similar method was used by Li et al. [34] to quantify [EMIm][NTf_2] IL in the polysulfone matrix. TGA results of the microcapsule after the acetone immersion test shows residue wt.% similar to that of the neat polysulfone confirming IL removal by the test. DSC curve, after the acetone immersion test, shows a complete disappearance of the peak at -3.4 °C indicating IL removal as seen in Fig. 9 (B), (D), and (F).

3.5. Solubility measurement

CO_2 sorption capacity of IL, PSF, and microcapsules were performed at a constant temperature of 45 ℃ and pressure of 4 bar (see Table 2). The direct use of IL for CO_2 capture is of limited interest due the high viscosity and solid precipitates. The micro-encapsulation technique of the IL in small, spherical shell of CO_2-permeable materials significantly improve the contact surface area of the IL and thus enhance the capture capacity [51]. CO_2 sorption capacity of the IL, PSF and, PSF-IL was 13.3, 39.2 mg CO_2/g and 46.1 mg CO_2/g respectively. The interaction of polar groups of PSF with CO_2 molecules is responsible for sorption capacity of the PSF [52,53]. The encapsulation strategy of the IL and metal oxides in the polymer shell improve the CO_2 sorption capacity. The moderate-strength quadruple-dipole intermolecular interaction of CO_2 with the ILs/metal oxide is responsible for the CO_2 sorption. Furthermore, ILs molecular structure contribute to create a larger free volume to accommodate more CO_2 molecules [54]. IL encapsulation promotes an increase in the available specific surface area to enhance CO_2 sorption rate [55,56]. The microcapsule with 2 wt% of iron oxide shows sorption capacity of 37.9 ± 2.1 mg CO_2/g which is very similar to that of pure PSF. Increasing the amount of iron oxide to 10 wt% and 15 wt% an increase in CO_2 sorption capacity to 52.9 ± 2.3 mg CO_2/g and 57.4 ± 1.9 mg CO_2/g (1.30 mmol CO_2/g) was observed respectively. The increase of 34 % and 47 % in the sorption capacity of the

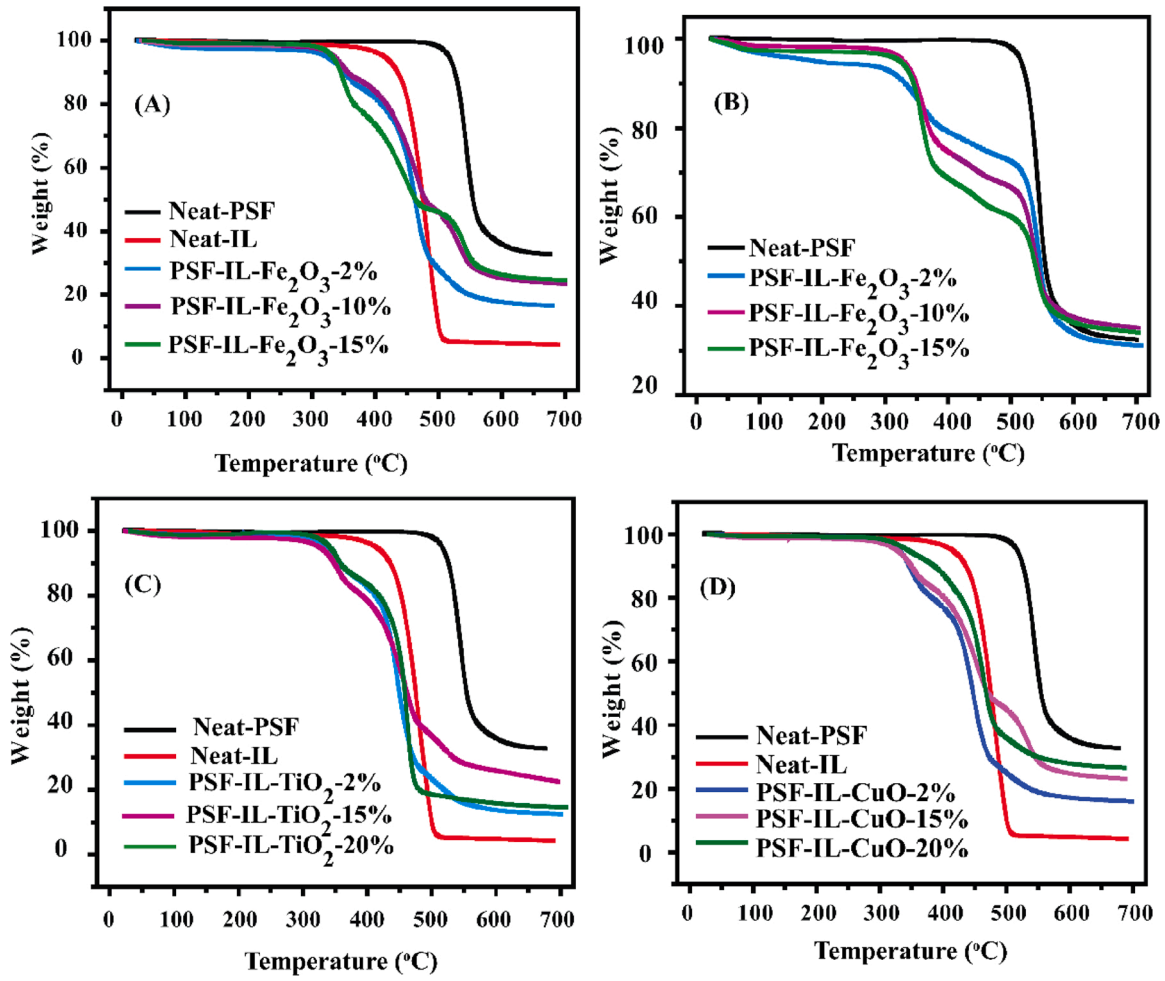

Fig. 7. (A) TGA curve of neat-PSF and microcapsule-containing Fe_2O_3, (B) TGA curve after acetone immersion test of microcapsule-containing Fe_2O_3, (C) TGA curve of neat-PSF and microcapsule-containing TiO_2, (D) TGA curve of neat-PSF and microcapsule-containing CuO.

Table 1
Result of thermal behavior of the microcapsule and TGA residue.

Samples	M (%)[a]	$T_{(onset)}$	$T_{(Max)}$	TGA Residue (%)[b]
Neat-PSF	0	525	545	0
Neat-IL	–	447	480	–
PSF-IL-Fe_2O_3-2%	2.0	323	463	2.5 ± 1.007
PSF-IL-Fe_2O_3-10%	10	326	463	4.9 ± 1.002
PSF-IL-Fe_2O_3-15%	15	347	447	9.4 ± 0.158
PSF-IL-TiO_2-2%	2.0	325	446	0.9 ± 0.623
PSF-IL-TiO2−15%	15	329	464	5.9
PSF-IL-TiO_2-20%	20	333	462	8.0 ± 0.335
PSF-IL-CuO-2%	2.0	324	446	3.4 ± 0.912
PSF-IL-CuO-15 %	15	324	452	7.3 ± 1.321
PSF-IL-CuO-20 %	20	339	462	10.1 ± 0.648

[a] Theoretic amount of metal oxide incorporated.
[b] The amount of the metal oxide calculated by TGA in air.

microcapsules containing 10 wt.% and 15 wt.% of the iron oxide respectively, reveal that the presence of an appropriate amount of metal ion have positive influence on CO_2 sorption capacity. Addition of TiO_2 (1.0 %) and CuO (20 %) shows CO_2 capture capacity of 46.10 mg CO_2/g and 48.19 mg CO_2/g respectively, presenting an improvement of 17 % and 22 % when compared to neat PSF, however, similar to the PSF-IL capsules (46.1 mg CO_2/g) and inferior when compared to samples with Fe_2O_3 addition. IL encapsulation capacity into the PSF shell (without metal oxide addition) is 48.6 %, around 34 % higher than IL with metal oxides encapsulation capacity. These results indicate that the samples with metal oxides (TiO_2 and CuO) addition present similar CO_2 sorption capacity that of PSF-IL but lower IL content. This result is essential for obtaining cost-effective materials, as metal oxides are low cost than the IL. In this work higher amounts of the iron oxide of 20 wt. % and 25 wt.% decreased the CO_2 sorption capacity from 57.4 ± 1.9 mg CO_2/g (15 % of Fe_2O_3) to 46.8 ± 1.58 mg CO_2/g and 44.3 ± 0.08 mg CO_2/g respectively, most probably due to the poor dispersion of the metal oxide above the optimal amount. It was concluded that the addition of up to 15 wt.% of the metal oxide (Fe_2O_3) favor the sorption capacity of the composite material. In our previous work we reported the bonding of the metal oxide (Fe_2O_3 and TiO_2) on the cellulose surface via hydroxyl group. The metal modified cellulose showed a significant enhancement in the CO_2 sorption uptake compared to non-modified cellulose [57]. Based on our previous experience and the results of the present work one can conclude that the presence of the metals oxides and their proper dispersion in the ionic liquid and polymer matrix can improve significantly CO_2 sorption capacity. It is clear from the Table 2 that the Fe_2O_3 shows the highest sorption capacity among the other oxides used in this work. Huang et al. [23] used the polyurea and alkylated graphene oxide IL capsule for CO_2 capture and reported an absorption capacity of 3.0 mg CO_2/g at a pressure of 1.3 bar. Ko et al. [58] immobilized primary, secondary and tertiary amines on mesoporous silica using as sorbent for CO_2 capture. The maximum capacity of primary, secondary, and tertiary amines supported silica was 0.95, 0.75, and 0.17 mmol CO_2/g respectively, whereas, our sample with 15 % of iron oxide achieved 1.30 mmol CO_2/g of sorption capacity. Santigo et al. [59] reported the encapsulation of three different IL

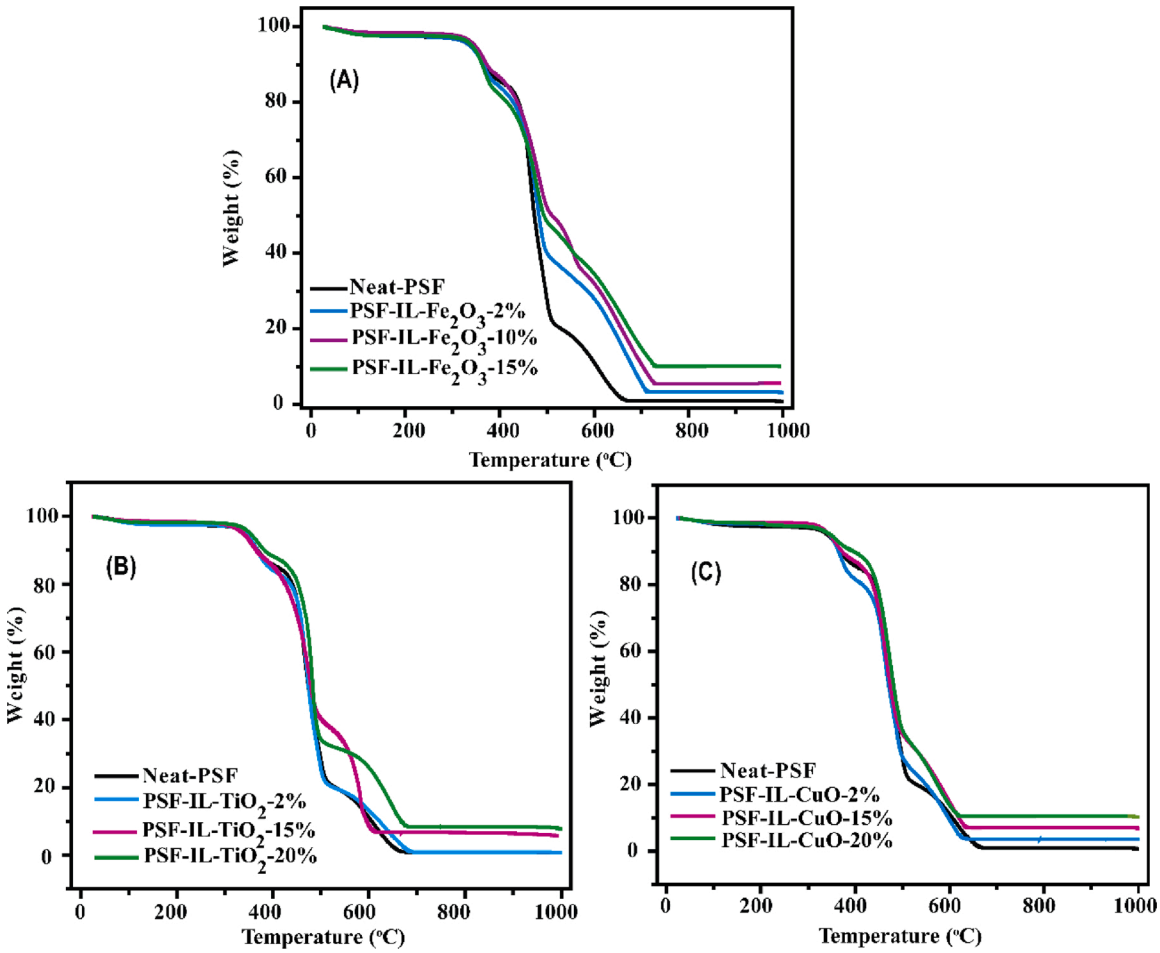

Fig. 8. TGA curve of neat-PSF and microcapsule in the air atmosphere.

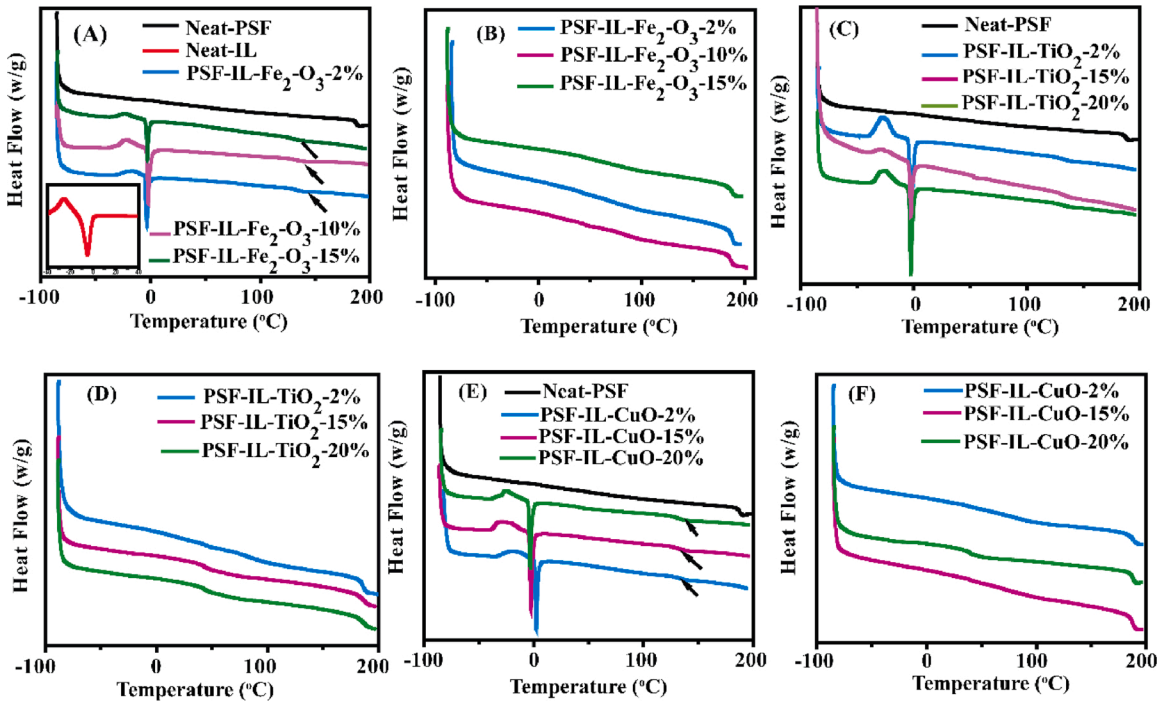

Fig. 9. DSC curve of neat-PSF and microcapsule containing different wt.% of the metal oxides before and after acetone immersion test, the inset in Figure (A) presents the curve of neat-IL.

Table 2
Result of encapsulation capacity and absorption of CO_2.

Samples	Filler (%)[b]	IL mass (%)	Sorption capacity mg CO_2/g
Neat-IL	–	–	14.3
Neat-PSF	–	–	39.2
PSF-IL	–	48.6 ± 0.6	46.1
PSF-IL-Fe_2O_3-2%	2.5	40.6 ± 0.4	37.9
PSF-IL-Fe_2O_3-10%	4.9	39.9 ± 0.32	52.9
PSF-IL-Fe_2O_3-15%	9.4	31.8 ± 0.84	57.4
PSF-IL-Fe_2O_3-20%	–	30.7 ± 0.63	46.8
PSF-IL-Fe_2O_3-25%	–	27.5 ± 0.93	44.3
PSF-IL-TiO_2-1%	0.7	35.5 ± 0.32	46.1
PSF-IL-TiO_2-2%	0.9	36.2 ± 0.21	41.8
PSF-IL-TiO_2-15%	5.9	33.3 ± 0.7	43.4
PSF-IL-TiO_2-20%	8.0	32.3 ± 0.51	44.5
PSF-IL-CuO-2%	3.4	32.4 ± 0.22	47.01
PSF-IL-CuO-10 %	–	34.9 ± 0.12	45.13
PSF-IL-CuO-15 %	7.3	34.8 ± 0.42	47.29
PSF-IL-CuO-20 %	10.1	36.9 ± 0.40	48.19

[b] The amount of the metal oxide calculated by TGA in air.

1-butyl-3-methylimidazolium prolinate [Bmim][PRO], 1-butyl-3-methylimidazolium methioinate [Bmim][MET], 1-butyl-3-methylimidazolium glycinate [Bmim][GLY] in porous carbon capsule. The CO_2 capture for [Bmim][PRO], [Bmim][MET], and [Bmim][GLY] encapsulated porous carbon capsule was 10 mg CO_2/g, 21 mg CO_2/g, and 24 mg CO_2/g respectively, at 1 bar of pressure and 333 K of temperature. Hence, their microcapsule shows improved sorption capacity compared to pure IL. They attributed this advance to the increase of the contact surface of the IL to the gas phase. The work of Kaviani et al. [60] showed 54 % and 41 % improvement in the CO_2 solubility at a pressure of 25 bar for [Emim][TF_2N] and [Hmim][TF_2N] respectively, encapsulated in a fluorine-containing polymer. In the present work, a similar behavior was observed at 4 bar of CO_2 pressure.

Here we introduced a new class of sorbent materials combining the advantages of both the liquid sorbent (such as high selectivity, water tolerance, and high capacity) and solid sorbent (for instant low volatile character and high surface area). CO_2 diffuses during sorption through the core shell interacting with the IL. The reverse reaction upon heating take place during the regeneration of high purity CO_2, which can successively be compressed for utilization or storage [61]. From the above results (Table 2) one can note that the samples with CuO present similar sorption capacity when compared with samples containing TiO_2 but inferior to that showed by the sample Fe_2O_3-15 wt.% (57.4 mg CO_2/g). This improved sorption capacity of the sample containing Fe_2O_3-15 wt. % is ascribed to the uniform and small size around 1 μm capsule formation. The lowered sorption capacity of the samples with CuO and TiO_2 compared to the Fe_2O_3 is probably attributed to the poor capsule formation and agglomerates as clearly showed from SEM and TEM images. Finally, the sorption/desorption test were carried out to assess the reusability of the material at 45 ℃ and 4 bar of CO_2 pressure. Fig. 10 shows the sorption/desorption test using the same sample (PSF-IL--Fe_2O_3-15 %) up to 6 cycles. The sample were regenerate by heating up to 70 ℃ at the end of each sorption test. The results prove that the sample retain the CO_2 sorption capacity up to 6 cycles showing the constancy of the material.

3.6. Justification of sorption performance via computer modeling

Simulations are routinely helpful in understanding multi-component systems. They allow to separate effects and, therefore, to precisely observe the most important phenomena. Fig. 11 shows binding energies for each component of the systems. D-metal nanoparticles are the most powerful CO_2 sorbents and this is confirmed by the sorption measurements discussed above (Table 2). Almost all systems reinforced by oxides particles perform better than metal-free sorbents. The identity of the metal does not matter essentially based on the calculated binding

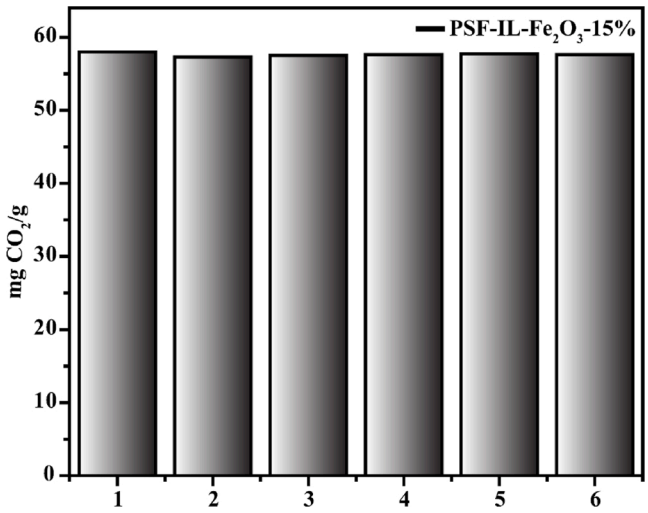

Fig. 10. CO_2 capture cycle of microcapsule (contains 15 wt.% Fe_2O_3) at 318.15 K and 4 bar.

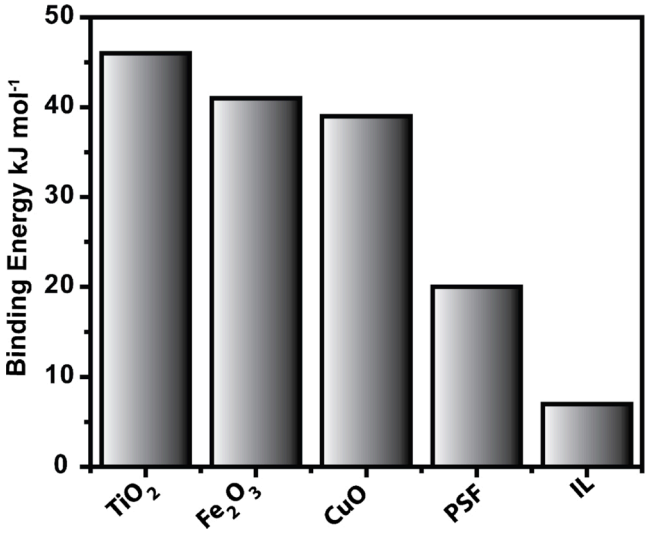

Fig. 11. Interaction energies of carbon dioxide with different species used in the composed sorption systems. Note that in all cases only physical adsorption (no carbonate anion formation) took place based on the experimental conditions.

energies. In fact, the reported energies are in direct proportion to the polarities of the nanoparticles based on the electronegativities of the atoms (1.63 for titanium, 1.88 for iron, 1.90 for copper). The strongest binding is seen in the case of TiO_2, whereas the weakest binding occurs in the case of CuO. Consider the trend in light of computed partial electrostatic charges: +0.49 at Fe, +0.41 at Cu, and +1.1 at Ti.

We did not find any significant difference in the binding of CO_2 to metal oxides. Therefore, the experimentally observed differences (Table 2) can only for rationalized in terms of different dispersion degrees in different sorbents measured, i.e. by the methods of preparation of these colloidal systems. While TiO_2 looks to be the best candidate for such sort of CO_2 scavengers, an ability to maximize its surface area is the key prerequisite of its successful implementation.

Adsorption of CO_2 on the inorganic oxides fragments occurs in the framework of Lewis acid-base theoretical description. Since the nature of interactions is the same, the performance of all three oxides is comparable. A final product of the reaction of acidic and basic oxides is a salt (carbonate). Nonetheless, the reactions could not proceed so far,

because proper heating was not attempted. The observed process is purely physical adsorption.

4. Conclusion

Thermally stable IL-metal oxide encapsulated in polysulfone shell microcapsules were successfully synthesized. The uniform microcapsule formation with very low agglomeration when iron oxide was used was corroborated from the TEM and SEM images. The microcapsules contain different metal oxides presented different average sizes as evidenced by SEM. The acetone immersion test shows around 27–40 % of the encapsulation capacity for the addition of different wt.% of metal oxide. The TGA analysis show a relative low initial degradation temperature for the microcapsule as compare to neat PSF. The DSC analysis of the core shell after the acetone immersion test shows a complete disappearance of characteristic peak of IL at -3.4 ℃ confirming the IL encapsulation. The microcapsule showed improved CO_2 absorption of around 47 % with the incorporation of 15 wt.% of iron oxide being attributed to the formation of small and uniform size capsule compared to CuO and TiO_2 samples. It was observed that all the systems having metal oxides performed better for CO_2 sorption compared to the systems without metal oxides. The simulations study showed the maximum interaction of the CO_2 with the TiO_2 followed by Fe_2O_3 and CuO. Our encapsulation process can be used for the encapsulation of various type of IL, in polymer shell combining with different metals, metal oxides and carbon based nanoparticle which can sufficiently improve CO_2 capture capacity. Thus, we report an easy approach to synthesize IL-PSF microcapsule in the presences of metal oxide for enhance CO_2 capture from the flue-gasses.

CRediT authorship contribution statement

Muhammad Nisar: Conceptualization, Methodology, Investigation. **Franciele L. Bernard:** Conceptualization, Investigation, Methodology, Project administration. **Evandro Duarte:** Investigation, Validation. **V. V. Chaban:** Conceptualization, Methodology, Investigation. **Sandra Einloft:** Conceptualization, Methodology, Project administration, Funding acquisition.

Declaration of Competing Interest

The authors report no declarations of interest.

Acknowledgment

The authors gratefully acknowledge support from Shell Brazil and the strategic importance of the support given by ANP (Brazil's National Oil, Natural Gas and Biofuels Agency) through the R&D levy regulation. Sandra Einloft thanks CNPq (National Council for Scientific and Technological Development) for research scholarship.

Appendix A. Supplementary data

Supplementary material related to this article can be found, in the online version, at doi:https://doi.org/10.1016/j.jece.2020.104781.

References

[1] C. hung Cheng, K. Li, H. Yu, K. Jiang, J. Chen, P. Feron, Amine-based post-combustion CO2capture mediated by metal ions: advancement of CO2desorption using copper ions, Appl. Energy 211 (2018) 1030–1038, https://doi.org/10.1016/j.apenergy.2017.11.105.

[2] E. Blomen, C. Hendriks, F. Neele, Capture technologies: improvements and promising developments, Energy Procedia 1 (2009) 1505–1512, https://doi.org/10.1016/j.egypro.2009.01.197.

[3] A.S. Bhown, B.C. Freeman, Analysis and status of post-combustion carbon dioxide capture technologies, Environ. Sci. Technol. 45 (2011) 8624–8632, https://doi.org/10.1021/es104291d.

[4] N. El Hadri, D.V. Quang, E.L.V. Goetheer, M.R.M. Abu Zahra, Aqueous amine solution characterization for post-combustion CO2capture process, Appl. Energy 185 (2017) 1433–1449, https://doi.org/10.1016/j.apenergy.2016.03.043.

[5] F. Shakerian, K.H. Kim, J.E. Szulejko, J.W. Park, A comparative review between amines and ammonia as sorptive media for post-combustion CO2capture, Appl. Energy 148 (2015) 10–22, https://doi.org/10.1016/j.apenergy.2015.03.026.

[6] B.E. Gurkan, J.C. De Fuente, E.M. Mindrup, L.E. Ficke, B.F. Goodrich, A. Price, W. F. Schneider, J.F. Brennecke, SI Equimolar CO 2 absorption by anion-functionalized ionic liquids Characterization, J. Am. Chem. Soc. 132 (2012) 2116–2117.

[7] S.B. Fredriksen, K.J. Jens, Oxidative degradation of aqueous amine solutions of MEA, AMP, MDEA, Pz: a review, Energy Procedia 37 (2013) 1770–1777, https://doi.org/10.1016/j.egypro.2013.06.053.

[8] E.S. Rubin, J.E. Davison, H.J. Herzog, The cost of CO2capture and storage, Int. J. Greenh. Gas Control. 40 (2015) 378–400, https://doi.org/10.1016/j.ijggc.2015.05.018.

[9] W. Luo, Q. Yang, W. Conway, G. Puxty, P. Feron, J. Chen, Evaluation and modeling of vapor-liquid equilibrium and CO2Absorption enthalpies of aqueous designer diamines for post combustion capture processes, Environ. Sci. Technol. 51 (2017) 7169–7177, https://doi.org/10.1021/acs.est.7b00379.

[10] Y. Zhang, D. Sachde, E. Chen, G. Rochelle, Modeling of absorber pilot plant performance for CO2 capture with aqueous piperazine, Int. J. Greenh. Gas Control. 64 (2017) 300–313, https://doi.org/10.1016/j.ijggc.2017.08.004.

[11] K. Li, H. Yu, M. Tade, P. Feron, J. Yu, S. Wang, Process modeling of an advanced NH $_3$ abatement and recycling technology in the ammonia-based CO $_2$ capture process, Environ. Sci. Technol. 48 (2014) 7179–7186, https://doi.org/10.1021/es501175x.

[12] F. Xu, H. Gao, H. Dong, Z. Wang, X. Zhang, B. Ren, S. Zhang, Solubility of CO2in aqueous mixtures of monoethanolamine and dicyanamide-based ionic liquids, Fluid Phase Equilib. 365 (2014) 80–87, https://doi.org/10.1016/j.fluid.2013.12.020.

[13] V. Jiménez, A. Ramírez-Lucas, J.A. Díaz, P. Sánchez, A. Romero, CO $_2$ capture in different carbon materials, Environ. Sci. Technol. 46 (2012) 7407–7414, https://doi.org/10.1021/es2046553.

[14] B. Dutcher, M. Fan, A.G. Russell, Amine-based CO2 capture technology development from the beginning of 2013-A review, ACS Appl. Mater. Interfaces 7 (2015) 2137–2148, https://doi.org/10.1021/am507465f.

[15] B. Gurkan, B.F. Goodrich, E.M. Mindrup, L.E. Ficke, M. Massel, S. Seo, T.P. Senftle, H. Wu, M.F. Glaser, J.K. Shah, E.J. Maginn, J.F. Brennecke, W.F. Schneider, Molecular design of high capacity, low viscosity, chemically tunable ionic liquids for CO2 capture, J. Phys. Chem. Lett. 1 (2010) 3494–3499, https://doi.org/10.1021/jz101533k.

[16] M.B. Shiflett, E.J. Maginn, The solubility of gases in ionic liquids, AIChE J. 63 (2017) 4722–4737, https://doi.org/10.1002/aic.15957.

[17] M. Aghaie, N. Rezaei, S. Zendehboudi, A systematic review on CO2 capture with ionic liquids: current status and future prospects, Renew. Sustain. Energy Rev. 96 (2018) 502–525, https://doi.org/10.1016/j.rser.2018.07.004.

[18] M.G. Cowan, D.L. Gin, R.D. Noble, Poly(ionic liquid)/Ionic liquid ion-gels with high "free" ionic liquid content: platform membrane materials for CO2/Light gas separations, Acc. Chem. Res. 49 (2016) 724–732, https://doi.org/10.1021/acs.accounts.5b00547.

[19] R. Santiago, J. Lemus, D. Moreno, C. Moya, M. Larriba, N. Alonso-Morales, M. A. Gilarranz, J.J. Rodríguez, J. Palomar, From kinetics to equilibrium control in CO2 capture columns using Encapsulated Ionic Liquids (ENILs), Chem. Eng. J. 348 (2018) 661–668, https://doi.org/10.1016/j.cej.2018.05.029.

[20] M. Mirzaei, B. Mokhtarani, A. Badiei, A. Sharifi, Improving physical adsorption of CO2 by ionic liquids-loaded mesoporous silica, Chem. Eng. Technol. 41 (2018) 1272–1281, https://doi.org/10.1002/ceat.201700314.

[21] J. Palomar, J. Lemus, N. Alonso-Morales, J. Bedia, M.A. Gilarranz, J.J. Rodriguez, Encapsulated ionic liquids (ENILs): from continuous to discrete liquid phase, Chem. Commun. (Camb.) 48 (2012) 10046–10048, https://doi.org/10.1039/c2cc35291e.

[22] J. Lemus, J. Bedia, C. Moya, N. Alonso-Morales, M.A. Gilarranz, J. Palomar, J. J. Rodriguez, Ammonia capture from the gas phase by encapsulated ionic liquids (ENILs), RSC Adv. 6 (2016) 61650–61660, https://doi.org/10.1039/c6ra11685j.

[23] Q. Huang, Q. Luo, Y. Wang, E. Pentzer, B. Gurkan, Hybrid ionic liquid capsules for rapid CO 2 capture, Ind. Eng. Chem. Res. 58 (2019) 10503–10509, https://doi.org/10.1021/acs.iecr.9b00314.

[24] M.C. Stern, F. Simeon, H. Herzog, T.A. Hatton, Post-combustion carbon dioxide capture using electrochemically mediated amine regeneration, Energy Environ. Sci. 6 (2013) 2505–2517, https://doi.org/10.1039/c3ee41165f.

[25] Y. Yu, T. Zhang, G. Liu, Z. Zhang, G. Wang, Identifying the multi-ion effects on the phase flow, mass and heat transfer in amine absorption of CO2, Int. J. Heat Mass Transf. 114 (2017) 501–516, https://doi.org/10.1016/j.ijheatmasstransfer.2017.06.048.

[26] G. Léonard, A. Voice, D. Toye, G. Heyen, Influence of dissolved metals and oxidative degradation inhibitors on the oxidative and thermal degradation of monoethanolamine in postcombustion CO2capture, Ind. Eng. Chem. Res. 53 (2014) 18121–18129, https://doi.org/10.1021/ie5036572.

[27] Z. Wang, W.A. Mitch, Influence of Dissolved Metals on N-Nitrosamine Formation under Amine-based CO2 Capture Conditions, Environ. Sci. Technol. 49 (2015) 11974–11981, https://doi.org/10.1021/acs.est.5b03085.

[28] S. Kumar, S.K. Saxena, A comparative study of CO2 sorption properties for different oxides, Mater. Renew. Sustain. Energy 3 (2014) 30, https://doi.org/10.1007/s40243-014-0030-9.

[29] J. Dupont, C.S. Consort, P.A.Z. Suarez, R.F. Souza, Preparation of 1-Butyl-3-Methyl imidazolium-based room temperature ionic liquids, Organic Synth. 79 (2002) 236, https://doi.org/10.15227/orgsyn.079.0236.
[30] S.S. Rao, S.P. Gejji, Electronic Structure, NMR, Spin–Spin Coupling, and Noncovalent Interactions in Aromatic Amino Acid Based Ionic Liquids, J. Phys. Chem. A 120 (2016) 5665–5684, https://doi.org/10.1021/acs.jpca.6b03985.
[31] K.A. Kurnia, T.E. Sintra, Y. Danten, M.I. Cabaço, M. Besnard, J.A.P. Coutinho, A simple method for preparation of a novel hydrophobic ionic liquid with a perfluoro-tert-butoxide anion, New J. Chem. 41 (2017) 47–50, https://doi.org/10.1039/C6NJ02575G.
[32] K. Noack, P.S. Schulz, N. Paape, J. Kiefer, P. Wasserscheid, A. Leipertz, The role of the C2 position in interionic interactions of imidazolium based ionic liquids: a vibrational and NMR spectroscopic study, Phys. Chem. Chem. Phys. 12 (2010) 14153, https://doi.org/10.1039/c0cp00486c.
[33] D.D. Ferreyra, N.M. Correa, J.J. Silber, R.D. Falcone, The effect of different interfaces and confinement on the structure of the ionic liquid 1-butyl-3-methylimidazolium bis(trifluoromethylsulfonyl)imide entrapped in cationic and anionic reverse micelles, Phys. Chem. Chem. Phys. 14 (2012) 3460, https://doi.org/10.1039/c2cp23481e.
[34] H. Li, Q. Wang, H. Wang, Y. Cui, Y. Zhu, B. Wang, Fabrication of thermally stable polysulfone microcapsules containing [EMIm][NTf2] ionic liquid for enhancement of in situ self-lubrication effect of epoxy, Macromol. Mater. Eng. 301 (2016) 1473–1481, https://doi.org/10.1002/mame.201600293.
[35] D.X. Chen, X.K. OuYang, Y.G. Wang, L.Y. Yang, D. Yu, Polysulfone microcapsules containing ionic liquid, Adv. Mater. Res. 554–556 (2012) 273–276, doi:10.4028/www.scientific.net/AMR.554-556.273.
[36] H. Li, Y. Cui, H. Wang, Y. Zhu, B. Wang, Preparation and application of polysulfone microcapsules containing tung oil in self-healing and self-lubricating epoxy coating, Colloids Surfaces A Physicochem. Eng. Asp. 518 (2017) 181–187, https://doi.org/10.1016/j.colsurfa.2017.01.046.
[37] R. Peverati, D.G. Truhlar, Performance of the M11 and M11-L density functionals for calculations of electronic excitation energies by adiabatic time-dependent density functional theory, Phys. Chem. Chem. Phys. 14 (2012) 11363–11370, https://doi.org/10.1039/c2cp41295k.
[38] P. Jeffrey Hay, Ab initio effective core potentials for molecular calculations. Potentials for K to Au including the outermost core orbitals, J. Chem. Phys. 82 (1985) 299.
[39] H. Grimme, S. Antony, J. Ehrlich, S. Krieg, A consistent and accurate ab initio parametrization of density functional dispersion correction (DFT-D) for the 94 elements H-Pu, J. Chem. Phys. 132 (2010) 154104.
[40] J.A. Schmidt, M.W. Baldridge, K.K. Boatz, J.A. Elbert, S.T. Gordon, M.S. Jensen, J. H. Koseki, S. Matsunaga, N. Nguyen, K.A. Su, S. Windus, T.L. Dupuis, M. Montgomery, General atomic and molecular electronic structure system, J. Comput. Chem. 14 (1993) 1347.
[41] Y. Ma, Z. Li, H. Wang, H. Li, Synthesis and optimization of polyurethane microcapsules containing [BMIm]PF6 ionic liquid lubricant, J. Colloid Interface Sci. 534 (2019) 469–479, https://doi.org/10.1016/j.jcis.2018.09.059.
[42] W.J. Koros, D.R. Paul, Design considerations for measurement of gas sorption in polymers by pressure decay, J. Polym. Sci.: Polym. Phys. Ed. 14 (1976) 1903–1907, https://doi.org/10.1002/pol.1976.180141014.
[43] W. Span, R. Wagner, A new EOS for CO2 covering the fluid region from the triple point temperature to 1100K at pressures up to 800MPa.pDf, J. Phys. Chem. Ref. Data 25 (1996) 1509–1596, https://doi.org/10.1063/1.555991.
[44] M. Day, J.D. Cooney, M. MacKinnon, Degradation of contaminated plastics: a kinetic study, Polym. Degrad. Stab. 48 (1995) 341–349, https://doi.org/10.1016/0141-3910(95)00088-4.
[45] P.K. Roy, P. Surekha, R. Raman, C. Rajagopal, Investigating the role of metal oxidation state on the degradation behaviour of LDPE, Polym. Degrad. Stab. 94 (2009) 1033–1039, https://doi.org/10.1016/j.polymdegradstab.2009.04.025.
[46] M. Nisar, C. Bergmann, J. Geshev, R. Quijada, G.B. Galland, An efficient approach to the preparation of polyethylene magnetic nanocomposites, Polym. (United Kingdom). 97 (2016) 131–137, https://doi.org/10.1016/j.polymer.2016.05.029.
[47] Luan, Ibuprofen-loaded poly(lactic-co-glycolic acid) films for controlled drug release, Int. J. Nanomedicine (2011) 659, https://doi.org/10.2147/IJN.S17011.
[48] R. Gao, M. Zhang, S.-W. Wang, R.B. Moore, R.H. Colby, T.E. Long, Polyurethanes containing an imidazolium diol-based ionic-liquid chain extender for incorporation of ionic-liquid electrolytes, Macromol. Chem. Phys. 214 (2013) 1027–1036, https://doi.org/10.1002/macp.201200688.
[49] X. Chen, Y. Xie, Y. Ling, J. Zhao, Y. Xu, Y. Tong, S. Li, Y. Wang, Ionic liquid crystal induced morphological control of solid composite polymer electrolyte for lithium-ion batteries, Mater. Des. 192 (2020) 108760, https://doi.org/10.1016/j.matdes.2020.108760.
[50] E. Rynkowska, K. Fatyeyeva, W. Kujawski, Application of polymer-based membranes containing ionic liquids in membrane separation processes: a critical review, Int. Rev. Chem. Eng. 34 (2018) 341–363, https://doi.org/10.1515/revce-2016-0054.
[51] J.K. Stolaroff, C. Ye, D.T. Nguyen, J. Oakdale, J.M. Knipe, S.E. Baker, CO2 absorption kinetics of micro-encapsulated ionic liquids, Energy Procedia 114 (2017) 860–865, https://doi.org/10.1016/j.egypro.2017.03.1228.
[52] A.A. Gabrienko, A.V. Ewing, A.M. Chibiryaev, A.M. Agafontsev, K.A. Dubkov, S. G. Kazarian, New insights into the mechanism of interaction between CO $_2$ and polymers from thermodynamic parameters obtained by in situ ATR-FTIR spectroscopy, Phys. Chem. Chem. Phys. 18 (2016) 6465–6475, https://doi.org/10.1039/C5CP06431G.
[53] D.L. Tomasko, H. Li, D. Liu, X. Han, M.J. Wingert, L.J. Lee, K.W. Koelling, A review of CO2 applications in the processing of polymers, Ind. Eng. Chem. Res. 42 (2003) 6431–6456, https://doi.org/10.1021/ie030199z.
[54] J. Palgunadi, J.E. Kang, M. Cheong, H. Kim, H. Lee, H.S. Kim, Fluorine-free imidazolium-based ionic liquids with a phosphorous-containing anion as potential CO2 absorbents, Bull. Korean Chem. Soc. 30 (2009) 1749–1754, https://doi.org/10.5012/bkcs.2009.30.8.1749.
[55] J.K. Stolaroff, C. Ye, J.S. Oakdale, S.E. Baker, W.L. Smith, D.T. Nguyen, C. M. Spadaccini, R.D. Aines, Microencapsulation of advanced solvents for carbon capture, Faraday Discuss. 192 (2016) 271–281, https://doi.org/10.1039/C6FD00049E.
[56] R.D. Aines, C.M. Spaddaccini, E.B. Duoss, J.K. Stolaroff, J. Vericella, J.A. Lewis, G. Farthing, Encapsulated solvents for carbon dioxide capture, Energy Procedia 37 (2013) 219–224, https://doi.org/10.1016/j.egypro.2013.05.105.
[57] S. Campbell, F.L. Bernard, D.M. Rodrigues, M.F. Rojas, L.Á. Carreño, V.V. Chaban, S. Einloft, Performance of metal-functionalized rice husk cellulose for CO2 sorption and CO2/N2 separation, Fuel. 239 (2019) 737–746, https://doi.org/10.1016/j.fuel.2018.11.078.
[58] Y.G. Ko, S.S. Shin, U.S. Choi, Primary, secondary, and tertiary amines for CO2 capture: designing for mesoporous CO2 adsorbents, J. Colloid Interface Sci. 361 (2011) 594–602, https://doi.org/10.1016/j.jcis.2011.03.045.
[59] R. Santiago, J. Lemus, C. Moya, D. Moreno, N. Alonso-Morales, J. Palomar, Encapsulated ionic liquids to enable the practical application of amino acid-based ionic liquids in CO2 capture, ACS Sustain. Chem. Eng. 6 (2018) 14178–14187, https://doi.org/10.1021/acssuschemeng.8b02797.
[60] S. Kaviani, S. Kolahchyan, K.L. Hickenbottom, A.M. Lopez, S. Nejati, Enhanced solubility of carbon dioxide for encapsulated ionic liquids in polymeric materials, Chem. Eng. J. 354 (2018) 753–757, https://doi.org/10.1016/j.cej.2018.08.086.
[61] J.J. Vericella, S.E. Baker, J.K. Stolaroff, E.B. Duoss, J.O. Hardin, J. Lewicki, E. Glogowski, W.C. Floyd, C.A. Valdez, W.L. Smith, J.H. Satcher, W.L. Bourcier, C. M. Spadaccini, J.A. Lewis, R.D. Aines, Encapsulated liquid sorbents for carbon dioxide capture, Nat. Commun. 6 (2015) 1–7, https://doi.org/10.1038/ncomms7124.